analytical chemistry

Article

pubs.acs.org/ac

A Simple Separation Method with a Microfluidic Channel Based on Alternating Current Potential Modulation

Hui-Bog Noh, Pranjal Chandra, You-Jeong Kim, and Yoon-Bo Shim*

Department of Chemistry and Institute of BioPhysio Sensor Technology, Pusan National University, Busan 609-735, South Korea

Supporting Information

ABSTRACT: A simple separation and detection system based on an electrochemical potential modulated microchannel (EPMM) device was developed for the first time. The application of alternating current (AC) potential to the microfluidic separation channel walls, which were composed of screen printed carbon electrodes, resulted in the oscillation and fluctuation of analytes and in the formation of a perfect flat flow front. These events resulted in an increase in the effective concentration and in the fine separation of samples. The performance of the EPMM device was examined through the analysis of endocrine disruptors (EDs) and heavy metal ions (HMIs) as model compounds. The analytical parameters that affected the separation and detection of EDs and HMIs were studied in terms of AC amplitude, AC frequency, flow rate, buffer concentration, pH, detection potential, and temperature. The separation efficiency was evaluated through measurements of the theoretical plate number (N), the retention time, and the half-peak width. Linear calibration plots for the detection of EDs and HMIs were obtained between 0.15 and 250.0 nM (detection limit 86.4 ± 2.9 pM) and between 0.01 and 10.0 nM (detection limit 9.5 ± 0.3 pM), respectively. The new device was successfully demonstrated with authentic and real samples.

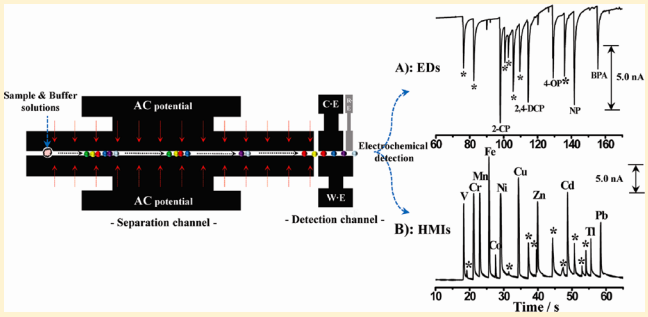

By the middle of the 20th century, the separation of chemicals was mainly performed by precipitation, distillation, and extraction. However, as chemicals became more diverse and complicated due to rapid industrialization, various separation techniques, including chromatography, capillary electrophoresis, and lab-on-a-chip, expanded the applicability of separation to several fields, such as the healthcare, medical, environmental science, materials science, and food science fields. Among these separation methods, chromatography has been extensively developed over the past 50 years,[1−3] which has consequently led to the development of gas,[4] liquid,[5] and supercritical-fluid[6] chromatographic techniques. Although chromatography has been frequently used because of its excellent separation capability for multiple components present in trace amounts, the long measuring time and easy changes in the experimental parameters cause deterioration of analytes. As a consequence, chromatography cannot be used for the separation of samples that exhibit instability or contain large analytes. In addition, the other conventional methods of electrophoresis,[7−9] capillary electrophoresis,[10−12] and field-flow fractionation (FFF)[13−15] were also developed chronologically for the efficient separation and detection of diverse samples including proteins, DNA, RNA, inorganic ions, and vitamins.

Recently, the micro-total analysis system (μ-TAS) technique has been successfully implemented in microfluidic devices for the separation of chemicals based on conventional electrophoretic[16−19] and pressure-flow microchannel devices.[20−25] In addition, other external fields or driving forces, such as the capillary effect, electric fields, magnetic fields, and rotation, have been reported for the separation of samples in microfluidic devices.[26] Along with these separation methods, the development of techniques that introduce electrochemical methodologies using a separation channel with porous Vycor glass with an electrode installed inside the channel tube has also been attempted.[27,28] The development of this technique was almost discontinued due to technical problems that arose with the porous separation channel. Thus, we attempted to develop a new separation technique using a microfluidic channel constructed with carbon electrodes that apply an alternating current (AC) potential to the channel walls. We refer to this technique as the electrochemical potential modulated microchannel (EPMM) system. This technique is different from those previously reported, where an AC potential was applied in the separation solution or at only few points along a single side of the channel wall and AC electroosmotic trapping.[29] No method similar to EPMM has been reported, where the AC potential is applied to the walls of two planar carbon electrodes that compose a channel. This EPMM device is expected to allow the rapid and simple separation of various chemicals and to improve the weaknesses of conventional separation methods. The application of an AC potential to the separation channel

Received: May 18, 2012
Accepted: October 17, 2012
Published: October 17, 2012

   dx.doi.org/10.1021/ac301351y | *Anal. Chem.* 2012, 84, 9738−9744

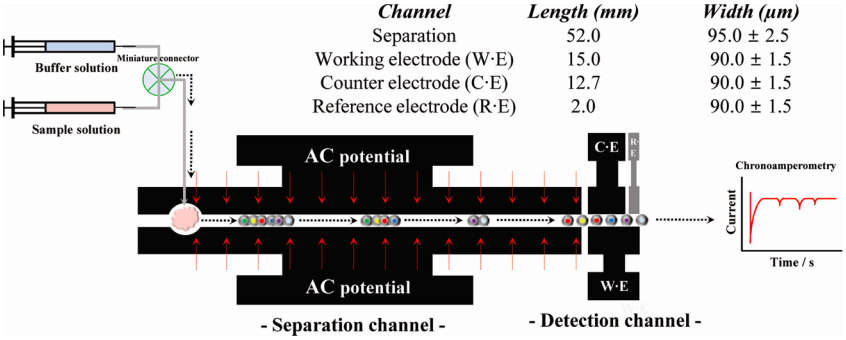

Figure 1. Schematic diagram of the experimental setup used to generate an AC electric field in the EPMM device.

wall allows control of the flow pattern to the flat flow front, which clearly enhances the separation efficiency.

In the present study, an EPMM device was fabricated using the screen printing technique, and the key experimental parameters that affect the separation efficiency, including the modulation potential, the flow rate, the frequency and amplitude of AC electric fields, and the flow pattern as a function of potential modulation, were evaluated with amperometry. To examine the separation performance of the EPMM device, several organic endocrine disruptors (EDs) and heavy metal ions (HMIs) were analyzed as model compounds. The analysis conditions were optimized to achieve the lowest detection limit, the widest dynamic rage, and the highest separation efficiency. The reliability of the EPMM device was examined through an analysis of real water samples.

EXPERIMENTAL SECTION

Materials. Microscope slide glasses were purchased from Natsunami (Japan). Carbon and silver inks were purchased from Juju Chemical (Japan). The endocrine disruptors (EDs; 2-chlorophenol (2-CP), 2,4-dichlorophenol (2,4-DCP), 4-octylphenol (4-OP), nonylphenol (NP), and bisphenol A (BPA)) were purchased from Sigma-Aldrich (USA). Heavy metal ions (HMIs; 1000.0 ppm Ni, Cu, Zn, Cd, and Pb) were purchased from Kanto Chemical (Japan). A phosphate buffer solution (PBS, pH 7.0) was prepared by mixing 0.1 M sodium dihydrogen phosphate with 0.1 M disodium hydrogen phosphate (Sigma-Aldrich, USA). An acetate buffer solution (pH 3.6) was prepared by mixing 0.1 M acetic acid with 0.1 M sodium acetate (Sigma-Aldrich). All aqueous solutions were prepared using double-distilled water, which was obtained from a Milli-Q water purification system (18 MΩ cm). All other chemicals were of extrapure grade.

Instruments. A function generator (GSI, Model Protek 9340, South Korea) was used to apply the AC electric field to the electrode within the EPMM. The flow pattern of the samples in the EPMM device was visualized using a microscope (SOMETECH Model MV-324, South Korea). The microchannel was fabricated using a Bando Industrial Model BS-450HT (South Korea) screen printing machine. The working, counter, and reference electrodes at the end of the separation channel were connected to a potentiostat/galvanostat (Kosentech PT-2, South Korea) for the electrochemical analyses. The pH of the buffer solution was measured using a multichannel pH meter, Kosentech, Model KST102A (South Korea). An inductively coupled plasma mass spectrometer (ICPMS) (Perkin-Elmer, ELAN DRC-e, USA) was used in low- and medium-resolution modes.

Fabrication of the EPMM Device and the Detection Procedure. The separation channel and detection electrodes of the EPMM device were prepared by screen printing of glass microslides using carbon ink. Prior to the fabrication of the microchannels, a mixture of carbon ink and solvent was prepared and allowed to mix for 24 h. A network of channels was designed using a computer-aided design software package (Autocad; AutoDesk, San Rafael, CA, USA). The stencil was designed by Senjin Tech (South Korea). Five layers of carbon and silver inks were screen printed onto a glass microslide to produce the channels. To stabilize the channel, soft baking and hard baking were performed for 1.0 h at 60.0 and 100.0 °C, respectively. Iron(III) chloride was dropped onto Ag to form a AgCl layer for the fabrication of the reference electrode. An additional epoxy film was coated using the screen printing system and then dried for 30 min at room temperature under vacuum. The microchannel was cleaned by flowing 0.1 M HCl through the system, followed by distilled water. The microchannel was dried at room temperature and then under vacuum. All slide glasses were washed with a cleaning solution prior to the printing process.

RESULTS AND DISCUSSION

Characteristics of the EPMM Device. The fabricated EPMM device for the separation and detection of analytes is shown in Figure 1. The length of the separation channel was 52.0 mm, and the working electrode was 15.0 mm in length. The lengths of the reference and counter electrodes were 2.0 and 12.7 mm, respectively. Figure S1 in the Supporting Information shows microphotographs of the inner dimensions of the device composed of (a) a separation part and (b) a detection part that consisted of a Ag/AgCl reference and a carbon working electrode (magnification 600×). The width of the separation channel was 95.0 ± 2.5 μm, and the width between the working and reference electrodes was 90.0 ± 1.5 μm. The thickness of the carbon ink printed onto the microscope slide was 15.0 ± 2.0 μm, as shown in Figure S1c in the Supporting Information. The in-channel electrochemical detector design produced fast and reproducible results and demonstrated an improvement over the external detection system. The buffer solutions were injected into the microchannel through a miniaturized automated microsyringe pump (Twins syringe pump Model-33, Harvard Apparatus, USA) followed by injection of 10.0 μL of the sample solutions (EDs and HMIs). The separation was performed according to the following procedure: after the sample was injected, the separation part of the EPMM device was connected to an AC generator and the AC potential was applied. The electric field produced a perturbation in the potential, which enhanced

dx.doi.org/10.1021/ac301351y | Anal. Chem. 2012, 84, 9738−9744

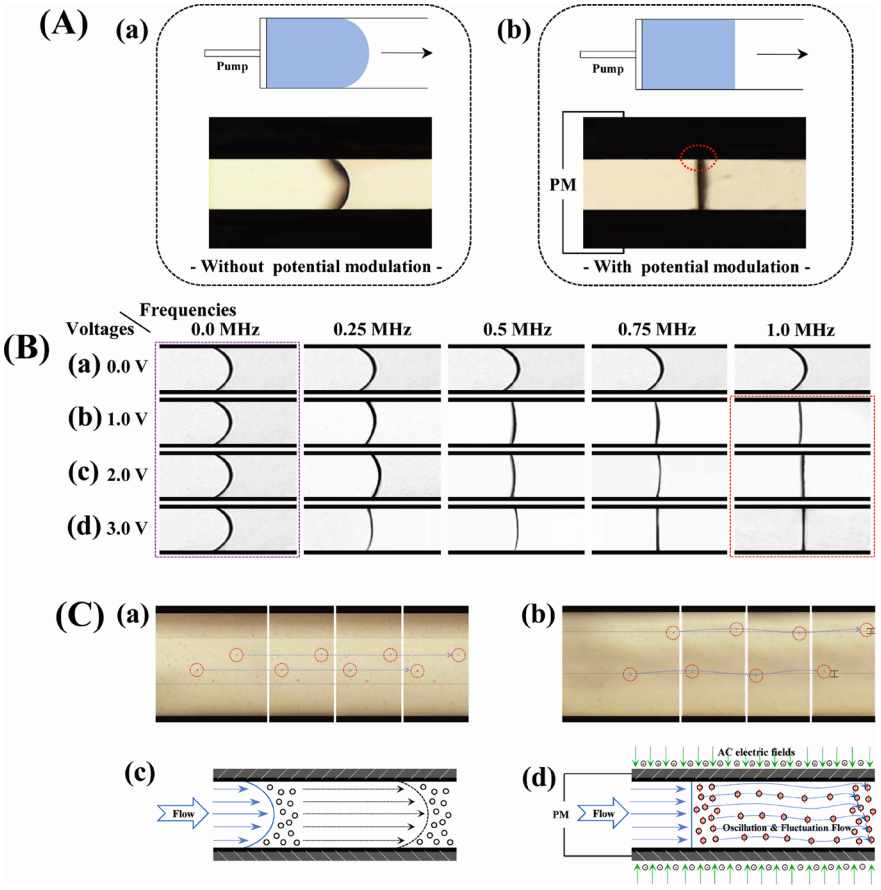

Figure 2. (A) Representative optical microscope images of the fluid movement profile at 600× magnification, (B) using voltages of (a) 0.0, (b) 1.0, (c) 2.0, and (d) 3.0 V and applied frequencies of 0.0, 0.25, 0.5, 0.75, and 1.0 MHz. (C) Microscopic images (a, c) without the AC potential application and (b, d) with the potential application. Profiles of (c) a parabolic front flow caused by hydrodynamic flow and (d) a flat front and potential modulated flow caused by application of the AC potential.

the separation efficiency. The samples were allowed to migrate through the separation channel according to their charge-to-mass ratio and were then collected at the detection electrodes, which were isolated from the end of the separation channel.

Microscopic images of flow patterns obtained in the absence and the presence of potential modulation are shown in Figure 2A. Without modulation of the potential, a typical parabolic liquid flow was observed in the pressure-driven mode because the flow velocity was maximized in the center of the channel and decreased near the wall of the channel until it became nearly zero at the wall due to frictional forces (Figure 2A(a)). Otherwise, the flat flow front of the fluid was observed with potential modulation as shown in Figure 2A(b). Figure 2B illustrates the front flow patterns as a function of the amplitude and frequency of the applied AC electric field. The same typical parabolic flow pattern was observed at 0.0 V as was observed in the absence of potential modulation (Figure 2B(a)). As the amplitude of the AC electric fields was increased to 1.0 V, the flow front became flat at AC frequencies greater than 1.0 MHz (Figure 2B(b–d)) and exhibited a fluctuation in the flow of the sample. As the amplitude of the AC electric field was increased, the flow front became flat more quickly at a specific frequency: at potentials greater than 2.0 V, a completely flat front flow was observed at 1.0 MHz, and at 3.0 V, a flat front flow was also observed at 0.75 MHz, although it was not completely flat. This optimization experiment reveals that the flattest front flow is observed at an amplitude of 1.0 V and a frequency of 1.0 MHz. The flat front flow might be generated due to the decrease in the thickness of the electrical double layers adjacent to the walls of the separation channel. The decreased thickness results in a decrease in the resistance against the flow on the walls, which contributes to the flat flow front and a fine resolution. To illustrate the flow pattern of the analytes during the separation where the AC potential was applied to the channel walls, movement of AgCl particles (diameter ~ 5.0 μm) was observed using an optical microscope (600×). Figure 2C shows the image frames captured during the movement of AgCl particles as a function of the separation time without (Figure 2C(a,c)) and with (Figure 2C(b,d)) an applied AC potential. The particles oscillated and fluctuated in the hydrodynamic flow when the AC potential was applied to the channel wall, as shown in Figure 2C(b,d). In contrast, the particles in the channel where an AC potential was not applied moved in a laminar flow profile. Based on these results, the degree of oscillation and fluctuation can be assumed to be affected by the atomic or molecular weights, which results in the separation of analytes in order of increasing molecular weight. In this case, small molecules fluctuate faster and large molecules fluctuate slower due to the different AC field strengths, which may significantly contribute to the separation efficiency. We hypothesize that the enhanced concentration factor was due to the AC field gradient between the channel walls and the center of the channel. Based on the AC field gradient, it is possible that more samples accumulate in the center of the

dx.doi.org/10.1021/ac301351y | *Anal. Chem.* 2012, 84, 9738–9744

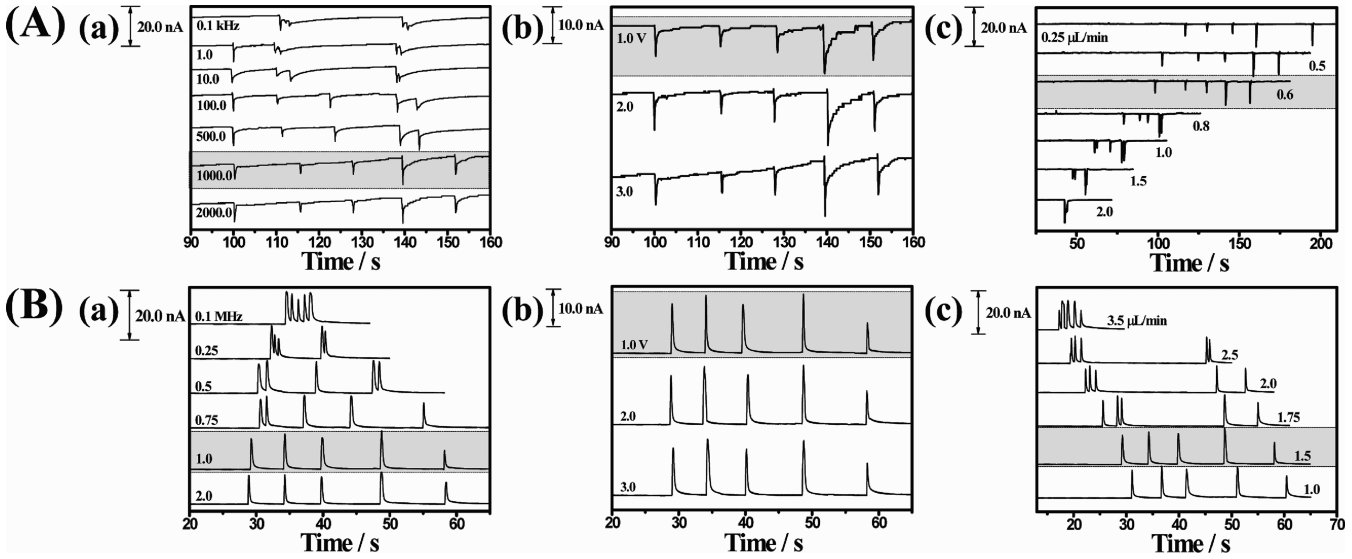

Figure 3. Effects of the (a) AC frequency, (b) AC amplitude, and (c) flow rate for (A) EDs and (B) HMIs. Concentration was 100.0 nM for all EDs and 1.5 nM for all HMIs.

channel, where the enhanced concentration efficiency was observed.

Analysis Potentials of Samples. To determine the appropriate potential for the detection of test samples, linear sweep voltammograms (LSVs) were recorded for the EDs and HMIs in a buffer solution at the detection electrode in the microchannel, as shown in Figure S2 in the Supporting Information. The LSVs show no oxidation peak for the (a) blank solution, whereas the EDs containing solution show oxidation peaks for 1.0 mM 2,4-DCP, 4-OP, 2-CP, BPA, and NP, as shown in (b), (c), (d), (e), and (f), respectively, of Figure S2 in the Supporting Information. The oxidation peaks of 2,4-DCP, 4-OP, 2-CP, BPA, and NP appeared at potentials of +657.7, +652.0, +680.3, +727.0, and +787.2 mV, and the magnitudes of the currents were +0.32, +0.36, +0.92, +1.15, and +1.20 μA, respectively. The peak current for NP was the highest due to its increased electrochemical activity.

Similarly, the detection potentials for the HMIs were also determined by recording LSVs for all the HMIs (Figure S2B in the Supporting Information). Reduction peaks were observed between −0.7 and −1.5 V in 0.1 M acetate buffer solution (pH 3.6) that contained the HMIs at a concentration of 1.0 mM. The LSVs in Figure S2B in the Supporting Information correspond to the (a) blank, (b) Pb, (c) Zn, (d) Cu, (e) Ni, and (f) Cd solutions. As expected, no reduction peaks were observed in the blank solution. Among all of the HMIs, the greatest peak current was observed for Cd because it exhibited the highest electrochemical activity. These results demonstrate that the EDs were completely oxidized at +1.0 V and that the HMIs were completely reduced at −1.5 V. Hence, the potentials of +1.0 and −1.5 V were applied to obtain a chronoamperometric response for detection of the EDs and HMIs, respectively, in the EPMM device.

Optimization of Separation and Detection Parameters. A successful separation and detection can be achieved when the movement of the solute occurs under optimal conditions. Therefore, the buffer concentration, pH, detection potential, temperature, and flow rate as well as the AC amplitude and AC frequency were optimized. The effect of the buffer concentration between 5.0 and 120.0 mM with respect to the current response of the EDs was studied (Figure S3A(a) in the Supporting Information). When the buffer concentration was increased from 5.0 to 60.0 mM, a gradual increase in the sensitivity was observed. At concentrations greater than 60.0 mM, the response decreased, possibly because of Joule heating, which might have become dominant at high buffer concentrations. Thus, the optimum buffer concentration was considered to be 60.0 mM. The effect of pH on the separation of the EDs was examined in the pH range of 6.0−8.0 at a detection potential of +1.0 V in 60.0 mM PBS (Figure S3A(b) in the Supporting Information). The oxidation currents of all of the EDs gradually increased as the pH increased from 6.0 to 7.0 and then decreased as the pH increased to 8.0. The maximum oxidation current was observed at pH 7.0. Accordingly, in the subsequent experiments, the pH of the buffer was maintained at 7.0. The effects of the detection potential on the electrochemical response of the EDs in the microfluidic channel were examined between +0.4 and +1.1 V. In this case, the current response increased from +0.4 to +1.0 V and then became almost constant (Figure S3A(c) in the Supporting Information). Accordingly, the subsequent experiments were performed at +1.0 V. The effect of temperature on the separation of EDs was investigated in the range between 10.0 and 50.0 °C. The electrochemical response increased gradually as the temperature was increased from 10.0 to 30.0 °C and then decreased when the temperature was further increased from 30.0 to 50.0 °C (Figure S3A(d) in the Supporting Information). On the basis of these temperature-response profiles, the optimum temperature was selected as 30.0 °C. To achieve the best separation of the EDs, the influence of the AC frequency was optimized in the range 0.1−2000.0 kHz. In the electrochromatograms obtained at 1000.0 kHz, five distinct peaks with different orders of migration were observed, as shown in Figure 3A(a). The amplitude of the AC electric field was also optimized at 1.0, 2.0, and 3.0 V. Figure 3A(b) shows the best separation of the ED mixture at 1.0 V. Thus, 1.0 V was used in the subsequent experiments. The flow rate was controlled with a syringe pump and was optimized to be in the range between 0.25 and 2.0 μL/min. At flow rates greater than 0.8 μL/min, complete separation was not observed. Indeed, complete

dx.doi.org/10.1021/ac301351y | Anal. Chem. 2012, 84, 9738−9744

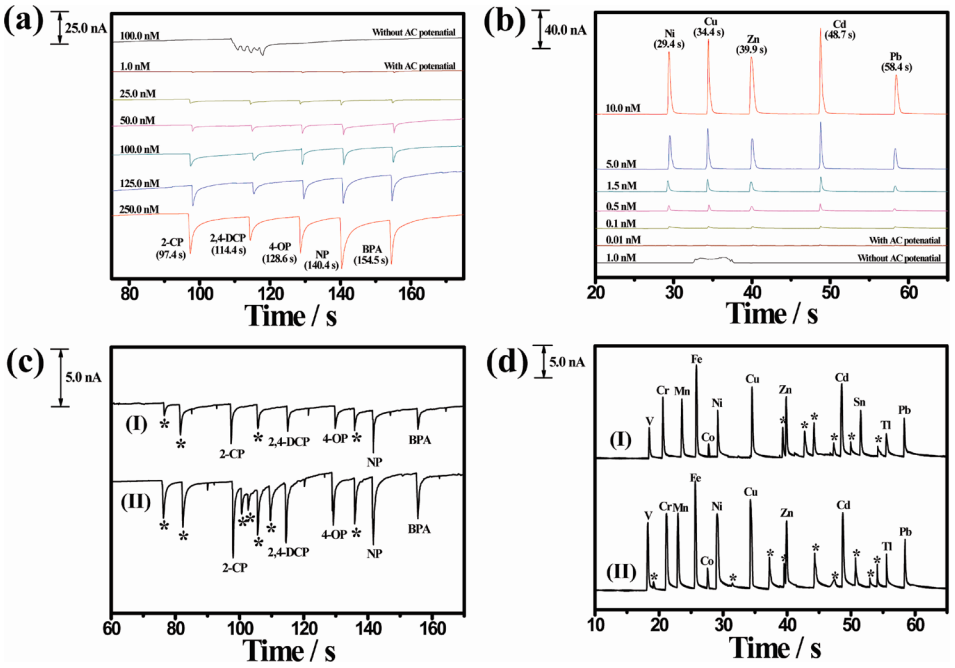

Figure 4. Electrochromatograms obtained for (a) EDs and (b) HMIs at different concentrations (EDs, 1.0−250.0 nM; HMIs, 0.01−10.0 nM). Electrochromatograms for the spiked concentration of (c) EDs and (d) HMIs in (I) tap and (II) surface water samples. The unknown chemical species detected in the real samples are indicated by asterisks.

separation was only achieved at flow rates of less than 0.6 μL/min, as shown in Figure 3A(c). The optimization of the experimental conditions results in an increase in the number of theoretical plates, which reduces the separation time and increases the separation ability.

We similarly optimized the experimental conditions for the separation and detection of the HMIs. For this purpose, the buffer concentration, pH, detection potential, temperature, flow rate, and AC frequency and amplitude were optimized. The buffer concentration was optimized for the analysis of HMIs between 5.0 and 50.0 mM. Maximum current was obtained at a concentration of 25.0 mM because of the previously discussed phenomenon (Figure S3B(a) in the Supporting Information). The effect of pH on the detection of HMIs was examined in the pH range 3.6−5.6 in a 25.0 mM acetate buffer solution. The pH dependence of the peak current in the electrochromatograms was investigated when HMIs were detected at different pH values (Figure S3B(b) in the Supporting Information). The peak current was maximized when a solution of acetate buffer with a pH of 3.6 was used; thus, this pH was used in the subsequent experiments. To obtain the maximum sensitivity, different potentials were examined for the detection of HMIs in the range −0.7 to −1.6 V, and the optimized potential was determined (Figure S3B(c) in the Supporting Information). The current response gradually increased as the detection potential was increased from −0.7 to −1.45 V and then remained unchanged at potentials greater than −1.45 V. For the complete reduction of the HMIs, a detection potential of −1.5 V was utilized for the detection of HMIs in the subsequent experiments. The temperature was also optimized in the range 10.0−50.0 °C. The maximum response was obtained at 25.0 °C (Figure S3B(d) in the Supporting Information); thus, this temperature was used in subsequent experiments for the detection of HMIs. For the best separation efficiency, the AC frequency was varied from 0.1 to 2.0 MHz. In the electrochromatogram obtained at 1.0 MHz, five distinct peaks were observed at different migration times as a function of the atomic weights of the HMIs, as shown in Figure 3B(a). In addition, the applied AC amplitude was also optimized at 1.0, 2.0, and 3.0 V. The best separation was achieved at an amplitude of 1.0 V, as shown in Figure 3B(b); thus, the amplitude of 1.0 V was used in the subsequent experiments. The flow rate was optimized in the range 1.0−3.5 μL/min. The best separation was observed at a flow rate of 1.5 μL/min, as shown in Figure 3B(c); thus, a flow rate of 1.5 μL/min was used in the subsequent experiments.

Separations using the EPMM Device. Having evaluated the performance of the microchannel detector, the system was utilized for the separation and detection of EDs and HMIs in the concentration ranges of 1.0−250.0 nM and 0.01−10.0 nM, respectively. As shown in Figure 4a, the response current for the separated species increased as the sample concentration was increased from 1.0 to 250.0 nM. The separation was completed within 154.5 (±1.2) s for all of the EDs. The migration times for 2-CP, 2,4-DCP, 4-OP, NP, and BPA were determined to be 97.4 (±0.6), 114.4 (±0.8), 128.6 (±1.0), 140.4 (±0.8), and 154.5 (±1.2) s, respectively, (k = 3, n = 5). The half-peak widths ($W_{1/2}$, the peak width at a half-maximum point) and the corresponding separation efficiencies (expressed as the number of theoretical plates, $N = 5.54(t_R/W_{1/2})^2$) for 2-CP, 2,4-DCP, 4-OP, NP, and BPA are presented in Table 1. Figure 4b shows the separation of the HMIs, where the current response increased as the concentration of the HMIs was increased from 0.01 to 10.0 nM. The separation of the HMIs was completed within 58.4 (±0.6) s. The migration times for the Ni, Cu, Zn, Cd, and Pb ions were 29.4 (±0.9), 34.4 (±0.5), 39.9 (±0.7), 48.7 (±0.5), and 58.4 (±0.6) s, respectively. The half-peak widths and corresponding separation efficiencies for Ni, Cu, Zn, Cd, and Pb are presented in Table 1.

Figure S4 in the Supporting Information shows the calibration curves obtained for the EDs and HMIs plotted as the peak current as a function of the sample concentrations.

dx.doi.org/10.1021/ac301351y | Anal. Chem. 2012, 84, 9738−9744

Table 1. Migration Times, Half-Peak Widths, and Separation Efficiencies for the EDs and HMIs Obtained Using the EPMM Method[a]

analyte		migration time (t_R, s)	half-peak width ($W_{1/2}$,[b] s)	N[c] (% RSD, n = 5)
endocrine disruptors	2-CP	97.4 ± 0.6	1.95 ± 0.41	13822 ± 691
	2,4-DCP	114.4 ± 0.8	1.85 ± 0.32	21185 ± 741
	4-OP	128.6 ± 1.0	1.81 ± 0.43	27966 ± 978
	NP	140.4 ± 0.8	1.27 ± 0.51	67707 ± 2106
	BPA	154.5 ± 1.2	1.42 ± 0.32	65583 ± 2229
heavy metal ions	Ni	29.4 ± 0.9	0.26 ± 0.01	70837 ± 2195
	Cu	34.4 ± 0.5	0.23 ± 0.02	123928 ± 3593
	Zn	39.9 ± 0.7	0.34 ± 0.05	76295 ± 2746
	Cd	48.7 ± 0.5	0.22 ± 0.02	271470 ± 7862
	Pb	58.4 ± 0.6	0.33 ± 0.03	173503 ± 5754

[a] n = 5. [b] Peak width at half-maximum point. [c] $N = 5.54(t_R/W_{1/2})^2$.

The dynamic range for the EDs was determined to be between 0.15 and 250.0 nM. The sensitivities obtained from the calibration plot were 1.958, 1.712, 1.849, 2.021, and 1.995 for 2-CP, 2,4-DCP, 4-OP, NP, and BPA, respectively. Table 2 summarizes the dynamic ranges, detection limits, and response precisions for the EDs and HMIs. The excellent reproducibility of this method confirms that the surface fouling of the microchannel detector is negligible. However, a slight variation in the migration times (relative standard deviation (RSD) < 5.5%, n = 5) was observed, which might be due to (i) changes in the concentration of the buffer and (ii) contamination of the walls of the channel caused by repetitive sample injections. The stability of the channel was examined using seven injections of 250.0 nM solutions of EDs. The samples were also analyzed during multiple injections; the RSD was <4.2% (n = 5), which indicated that the method was highly reproducible. The calibration plots for 2-CP, 2,4-DCP, 4-OP, NP, and BPA were found to be linear (with a correlation coefficient between 0.9913 and 0.9982) in the concentration range 0.15−250.0 nM, with detection limits of 202.5 (±7.8), 281.5 (±11.5), 230.8 (±8.5), 86.4 (±2.9), and 180.2 (±6.9) pM, respectively, based on a signal-to-noise ratio (S/N) of 3 (95% confidence level, k = 3, n = 5). These detection limits were significantly lower than those obtained by other groups who used liquid phase microextraction,[30] flow injection,[31] and field-amplified sample injection (FASI) analytical methods[32] and were comparable to those obtained using the solid phase extraction[33] and HPLC methods.[34]

Table 2. Analytical Performance of the Method

analytes		dynamic range (nM)	detection limit[a] (pM)	response precision (% RSD, n = 5)
endocrine disruptors	2-CP	0.50−250.0	202.5 ± 7.8	4.1
	2,4-DCP	0.85−250.0	281.5 ± 11.5	5.4
	4-OP	0.75−250.0	230.8 ± 8.5	4.3
	NP	0.15−250.0	86.4 ± 2.9	3.1
	BPA	0.25−250.0	180.2 ± 6.9	3.7
heavy metal ions	Ni	0.020−10.0	16.1 ± 0.5	3.2
	Cu	0.015−10.0	10.5 ± 0.4	2.4
	Zn	0.020−10.0	16.4 ± 0.5	2.2
	Cd	0.010−10.0	9.5 ± 0.3	2.3
	Pb	0.025−10.0	20.5 ± 0.8	2.3

[a] Estimated detection limits, based on S/N = 3.

The HMIs were similarly analyzed, and the dynamic ranges, the detection limit, and the precision of the method are summarized in Table 2. The dynamic range of the HMIs was determined to be between 0.01 and 10.0 nM. The sensitivities obtained from the calibration plot were 1.25, 1.27, 1.28, 1.25, and 1.38 for the Ni, Cu, Zn, Cd, and Pb ions, respectively. The calibration plots for the Ni, Cu, Zn, Cd, and Pb ions were linear in the concentration range 0.01−10.0 nM, with detection limits of 16.1 (±0.5), 10.5 (±0.4), 16.4 (±0.5), 9.5 (±0.3), and 20.5 (±0.8) pM, respectively, based on a S/N ratio of 3 (98% confidence level, k = 3, n = 5). The detection limit of the EPMM method (DL = 0.0095−0.0205 ppb) is therefore significantly lower than that of the ICPMS method (DL = 0.01−1.00 ppb). These results clearly indicate that the developed method is highly sensitive and selective for the detection of trace quantities of EDs and HMIs. The highest $[N]$ value of the EPMM device was 271 470 compared with the $[N]$ value of the PEG coated microfluidic device in a pressure driven flow mode, which was 35 082[35] for the separation and detection of fluorescent dye mixture, peptide and proteins, and also with that of the pressure driven microfabricated liquid chromatographic analyzer,[36] which was 5000 for the separation and detection of two food dyes. This clearly shows the better performance of the EPMM device compared with other separation techniques.

Analyses of Real Samples. To evaluate the reliability of the EPMM device, analyses of EDs and HMIs in real water samples were performed. Figure 4 shows the electrochromatograms for real samples of the (Figure 4c) EDs and (Figure 4d) metal ions, respectively. The real samples were collected from (I) a local tap water source (water service pipes, Pusan National University) and (II) local surface water (upper stream of a local canal), and the presence of EDs and metal ions was analyzed using the EPMM method. The peaks in Figure 4c were confirmed by the spiking of the water samples with standard solutions of phenols (5.0−10.0 nM). As demonstrated by electrochromatogram I in Figure 4c, several ED peaks in the tap water samples were confirmed using the standard compounds even though the obtained concentrations were less than the minimum hazardous levels.[37] For the surface water samples, the peaks were well separated from one another and were detected within migration times similar to those of the tap water samples, as shown in Figure 4, electrochromatogram II.[18] The average recoveries (n = 3) for all of the EDs in the tap and surface water samples were between 70 and 86% and between 76 and 89%, respectively, and the variations in the coefficients were 12−15% and 13−17%, respectively. However, in addition to these target peaks, other peaks were observed in both of the electrochromatograms, possibly because of the presence of other trace phenolic compounds in the water samples that are detected by the EPMM device. Thus, this method can be used for the rapid analysis of water samples that are suspected to be contaminated with phenolic compounds.

In a control experiment, the concentration of the HMIs in the real samples (tap water and surface water) was also analyzed using the ICPMS method. The latter method confirmed the presence of 20 ions (Li, Be, Ti, V, Cr, Mn, Fe,

dx.doi.org/10.1021/ac301351y | Anal. Chem. 2012, 84, 9738−9744

Co, Ni, Cu, Zn, As, Se, Sr, Mo, Cd, Sn, Sb, Tl, and Pb ions) in the concentration ranges of 0.11−18.57 μg/L for the tap water and 0.15−27.31 μg/L for the surface water. Figure 4d provides the electrochromatograms for the heavy metal ions in the (I) tap and (II) surface water samples. Furthermore, 16 of the 20 species detected by ICPMS were detected at −1.5 V by the EPMM device, where the ions were detected in the order of their atomic numbers: V, Cr, Mn, Fe, Co, Ni, Cu, As, Se, Mo, Zn, Cd, Sn, Sb, Tl, and Pb ions. The four metal ions that were not detected by the EPMM device were Li, Be, Ti, and Sr ions, which exhibit reduction potentials of E° = −3.05, −1.85, −1.63, and −2.89 V, respectively. These metal ions were not detected because these potentials are all greater than the reduction potential of −1.5 V applied in the EPMM device. As shown by curves I and II in Figure 4d, the separated peaks of the 16 ions present in the (I) tap water and (II) surface water samples were confirmed with the standard samples. The order of separated metal ions was consistent with the results of the ICPMS method. In addition, two and six foreign peaks were observed in (I) tap water and (II) surface water, respectively, which were not detected by the ICPMS method. This finding indicates that the EPMM method is capable of detecting nonmetal species that are reducible at −1.5 V.

CONCLUSIONS

The electrochemical AC potential modulation on a microfluidic channel resulted in the enhanced in situ concentration and separation by the oscillation and fluctuation of analytes in the flow of test samples. This method was successfully validated through the analysis of trace amounts of complex analytes in water samples. The separation and detection capabilities of the method based on the EPMM device were proven to be powerful and to afford the simultaneous detection of trace analytes. The developed method showed better sensitivity than the ICPMS method for analytes used in the present study and was also able to detect the analytes in real samples. These features indicate that this new method may be extended for diverse chemical and biochemical analyses.

ASSOCIATED CONTENT

Supporting Information

Additional figures showing microscopic images, LSV curves, optimization of detection parameters, and calibration curves. This material is available free of charge via the Internet at http://pubs.acs.org.

AUTHOR INFORMATION

Corresponding Author

*Tel.: +82-51-510-2244. Fax: +82-51-514-2430. E-mail: ybshim@pusan.ac.kr.

Notes

The authors declare no competing financial interest

ACKNOWLEDGMENTS

This work was supported by an NRF grant funded by the MEST, South Korea (Grant 20100029128).

REFERENCES

(1) Ettre, L. S.; Sakodynskii, K. I. *Chromatographia* **1993**, *35*, 223−231.
(2) Martin, A. J. P. In *Nobel Lectures: Chemistry 1942−1962*; Elsevier: Amsterdam, 1952; pp 359−371.
(3) Synge, R. L. M. In *Nobel Lectures: Chemistry 1942−1962*; Elsevier: Amsterdam, 1964; pp 374−387.
(4) Nogare, S. D. *Anal. Chem.* **1962**, *34*, 35−47.
(5) Snyder, L. R.; Kirkland, J. J.; Dolan, J. W. *Introduction to Modern Liquid Chromatography*; John Wiley & Sons: Hoboken, NJ, 2009.
(6) Gere, D. R. *Science* **1983**, *222*, 253−259.
(7) Jorgenson, J. W.; Phillips, M. *New Directions in Electrophoretic Methods*; American Chemical Society: Washington, DC, 1987; Chapter 1.
(8) Longsworth, L. G.; MacInnes, D. A. *Chem. Rev.* **1939**, *24*, 271−287.
(9) Slater, G. W.; Kist, T. B. L.; Ren, H.; Drouin, G. *Electrophoresis* **1998**, *19*, 1525−1541.
(10) Weinberger, R. *Practical Capillary Electrophoresis*; Academic Press: San Diego, CA, 1993.
(11) Sovocool, G. W.; Brumley, W. C.; Donnelly, J. R. *Electrophoresis* **1999**, *20*, 3297−3310.
(12) Wang, J. *Electroanalysis* **2005**, *17*, 1133−1140.
(13) Giddings, J. C. *Sep. Sci.* **1966**, *1*, 123−125.
(14) Schimpt, M. E.; Caldwell, K.; Gidding, J. C. *Field-Flow Fractionation Handbook*; John Wiley & Sons: New York, 2000.
(15) Gidding, J. C. *Sep. Sci.Technol.* **1984**, *19*, 831−847.
(16) Manz, A.; Graber, N.; Widmer, H. M. *Sens. Actuators, B: Chem.* **1990**, *1*, 244−248.
(17) Tüdos, A. J.; Besselink, G. A. J.; Schasfoort, R. B. M. *Lab Chip* **2001**, *1*, 83−95.
(18) Shiddiky, Md. J. A.; Park, H.; Shim, Y.-B. *Anal. Chem.* **2006**, *78*, 6809−6817.
(19) Shiddiky, Md. J. A.; Shim, Y.-B. In *Microfluidic Devices in Nanotechnology*; Kumar, C. S., Ed.; John Wiley & Sons: Hoboken, NJ, 2010; Chapter 6.
(20) Bai, X.; Josserand, J.; Jensen, H.; Rossier, J. S.; Girault, H. H. *Anal. Chem.* **2002**, *74*, 6205−6215.
(21) Dutta, D.; Ramsey, J. M. *Lab Chip* **2011**, *11*, 3081−3088.
(22) Crabtree, H. J.; Cheong, E. C. S.; Tilroe, D. A.; Backhouse, C. J. *Anal. Chem.* **2001**, *73*, 4079−4086.
(23) Crevillen, A. G.; Pumera, M.; Gonzaleza, M. C.; Escarpa, A. *Lab Chip* **2009**, *9*, 346−353.
(24) Lacher, N. A.; Lunte, S. M.; Martin, R. S. *Anal. Chem.* **2004**, *76*, 2482−2491.
(25) Dutta, D.; Leighton, D. T., Jr. *Anal. Chem.* **2001**, *73*, 504−513.
(26) Stone, H. A.; Stroock, A. D.; Ajdari, A. *Annu. Rev. Fluid Mech.* **2004**, *36*, 381−411.
(27) Davis, J. M.; Fan, F.-R. F.; Bard, A. J. *Anal. Chem.* **1987**, *59*, 1339−1348.
(28) Vandaveer, W. R., IV; Pasas-Farmer, S. A.; Fischer, D. J.; Frankenfeld, C. N.; Lunte, S. M. *Electrophoresis* **2004**, *25*, 3528−3549.
(29) Wu, J.; Ben, Y.; Chang, H.-C. *Anal. Chem.* **2005**, *1*, 161−167.
(30) Liu, J.-F.; Chi, Y.-G.; Jiang, G.-B.; Tai, C.; Peng, J.-F.; Hu, J.-T. *J. Chromatogr., A* **2004**, *1026*, 143−147.
(31) Gil, E. P.; Tang, H. T.; Halsall, H. B.; Helneman, W. R.; Misiego, A. S. *Clin. Chem.* **1990**, *36*, 662−665.
(32) Zhu, L.; Tu, C.; Lee, H. K. *Anal. Chem.* **2001**, *73*, 5655−5660.
(33) Buchholz, K. D.; Pawllszyn, J. *Anal. Chem.* **1994**, *66*, 160−167.
(34) Martinez, D.; Pocurull, E.; Marce, R. M.; Borrull, F.; Calull, M. *Chromatographia* **1996**, *43*, 619−624.
(35) Reschke, B. R.; Schiffbauer, J.; Edwards, B. F.; Timperman, A. T. *Analyst* **2010**, *135*, 1351−1359.
(36) Vahey, P. G.; Park, S. H.; Marquardt, B. J.; Xia, Y.; Burgess, L. W.; Synovec, R. E. *Talanta* **2000**, *51*, 1205−1212.
(37) Petrovic, M.; Eljarrat, E.; Lopez de Alda, M. J.; Barcelo, D. *Anal. Bioanal. Chem.* **2004**, *378*, 549−562.